

Indirect reciprocity as a dynamics for weak balance

Minwoo Bae¹ and Seung Ki Baek^{2,*}

¹*Research Institute for Basic Sciences,
Pukyong National University, Busan 48513, Korea*

²*Department of Scientific Computing,
Pukyong National University, Busan 48513, Korea*

Abstract

A social network is often divided into many factions. People are friends within each faction, while they are enemies of the other factions, and even my enemy's enemy is not necessarily my friend. This configuration can be described in terms of a weak form of structural balance. Although weak balance explains a number of real social networks, which dynamical rule achieves it has remained unexplored. In this work, we show that the answer can be found in the field of indirect reciprocity, which assumes that people assess each other's behavior and choose how to behave to others based on the assessment according to a social norm. We begin by showing that weak structural balance is equivalent to stationarity when the rule is given by a norm called 'judging'. By analyzing its cluster dynamics of merging, division, and migration induced by assessment error in complete graphs, we obtain the cluster size distribution in a steady state, which shows the coexistence of a giant cluster and smaller ones. We compare this shape with the distributions of seats among the parties in the parliaments of Germany, the United Kingdom, and Spain. This study suggests that indirect reciprocity can provide insight into the interplay between a norm that individuals abide by and the macroscopic group structure in society.

* seungki@pknu.ac.kr

I. INTRODUCTION

Judgmental thinking seems to be a universal instinct that most of us are born with. Even infants evaluate each other's behavior [1], and their judgment is so broad and conclusive that when they see someone violate moral principles, their inference easily jumps to the wrongdoer's moral character itself [2]. In the field of indirect reciprocity [3–7], researchers have used a mathematical characterization of judgmental behavior, according to which a norm called ‘judging’ is defined as in Table I: As the name indicates, judging bears a high degree of similarity to ‘stern judging’ [8–10], which says that one should not help the bad, but only the good. When it comes to judging, its difference from stern judging is that a bad donor's defection against a bad recipient is again judged as bad, which means that my enemy's enemy is not necessarily my friend. Thus, it should not be surprising that judging tends to create enemies rather than friends. This norm of judgment has been regarded as relatively marginal due to its poor performance in promoting cooperation when the assessment is private [7, 11, 12]. However, if we accept it as the *status quo*, this norm exhibits notable consequences at macroscopic scales, which could even have practical implications, and this is our point of view throughout this work.

It is already known that the dynamics of stern judging becomes stationary if and only if Heider's structural balance [13] is achieved [14–16]. According to the structure theorem [17, 18], a balanced configuration consists of two antagonistic groups, within each of which the individuals are positively related. Balance theory can therefore explain, for example, how two allied forces form in the case of warfare [19]. However, except for such an extreme conflict, a weak version of structural balance [20] is more favored on social networks [21–23], and the weak balance is obtained by relaxing the condition that my enemy's enemy is my friend. The corresponding weak version of the structure theorem states that every vertex in the graph can distinguish its friends and enemies without ambiguity if and only if the graph has no cycle with exactly one negative link [20]. Essentially, it means that a weakly balanced configuration consists of an arbitrary number of antagonistic groups. However, how to achieve weak balance through a dynamical rule remains unexplored, when compared with the extensive studies on Heider's original balance concept [24–27].

In this work, we will show that judging provides the rule that organizes a weakly balanced configuration. To our knowledge, this is the first report on a dynamical process to achieve

TABLE I. Characterization of judging, also known as L8 [28]. An observer observes an interaction between a donor and a recipient, where the donor may choose between cooperation (C) and defection (D). The observer assesses the donor in the following way: The observer’s updated assessment α_{uXv} is either good (G) or bad (B), depending on the observer’s existing assessment of the donor ($u \in \{G, B\}$), the donor’s behavior to the recipient ($X \in \{C, D\}$), and the observer’s assessment of the recipient ($v \in \{G, B\}$). The behavioral rule β_{uv} tells the donor to choose C or D depending on the donor’s self-assessment u and the donor’s assessment of the recipient v . Note that this norm has $\alpha_{BDB} = B$, differently from stern judging.

	α_{GCG}	α_{GDG}	α_{GCB}	α_{GDB}	α_{BCG}	α_{BDG}	α_{BCB}	α_{BDB}	β_{GG}	β_{GB}	β_{BG}	β_{BB}
Judging (L8)	G	B	B	G	G	B	B	B	C	D	C	D

weak balance despite its ubiquity in real social networks. To escape from a weakly balanced configuration, we introduce an assessment error which induces transitions among weakly balanced configurations with well-defined probabilities. By calculating the probabilities, we obtain a coarse-grained description of the judging dynamics at the group level, that is, how groups divide, merge, and exchange their members. The resulting steady-state distribution of group sizes shows a macroscopic consequence of the judging norm and can be compared with group structures in empirical data.

II. MODEL

Consider a complete directed graph of N vertices. Each vertex corresponds to an individual agent, and the link from a vertex i to another vertex j represents the assessment of j by i , which can be good or bad. At each time step, we choose a random pair of vertices as a donor and a recipient, respectively. Every individual has the same probability of being a donor, and it is also true for a recipient. The donor and recipient can be the same individual, but this probability is negligible when N is large. The donor chooses cooperation or defection to the recipient, depending on how it assesses themselves (see β_{uv} in Table I). All individuals in the population observe the interaction between the donor and the recipient to assess the donor according to the judging norm (see α_{uXv} in Table I). With a small probability ϵ , an observer’s assessment of the donor can be flipped from good to bad and vice versa.

III. RESULTS

A. Equivalence between stationarity and weak balance

To prove the equivalence between weak balance and stationarity, we map good (G) and cooperation (C) to $+1$, as well as bad (B) and defection (D) to -1 . Then, the updating rule in Table I can be summarized as

$$\sigma'_{od} = \frac{1}{4}(\sigma_{od}\sigma_{dr}\sigma_{or} - \sigma_{od}\sigma_{dr} - \sigma_{od}\sigma_{or} + 3\sigma_{dr}\sigma_{or} + \sigma_{od} + \sigma_{dr} + \sigma_{or} - 1), \quad (1)$$

where $\sigma_{ij} = \pm 1$ is a dynamic variable assigned to every link, say, from vertex i to j , for representing player i 's assessment of j , together with σ'_{ij} for denoting its updated value, and the subscripts o , d , and r mean an observer, a donor, and a recipient, respectively. If $\sigma_{ij} = +1$, the link from i to j is called positive, while $\sigma_{ij} = -1$ means that the link is negative. In stationarity, we must have $\sigma_{ij} = \sigma'_{ij}$, which imposes the following constraint:

$$\sigma_{ij} = \frac{1}{4}(\sigma_{ij}\sigma_{jk}\sigma_{ik} - \sigma_{ij}\sigma_{jk} - \sigma_{ij}\sigma_{ik} + 3\sigma_{jk}\sigma_{ik} + \sigma_{ij} + \sigma_{jk} + \sigma_{ik} - 1), \quad (2)$$

for every triad of vertices i , j , and k . Let us define a detector function for weak balance as follows:

$$\begin{aligned} W(x, y, z) &\equiv \frac{1}{2} \left[(1 + xyz) + \frac{1}{2}(1 - xyz)(xy + zx + yz - 1) \right] \\ &= \begin{cases} -1 & \text{if } (x, y, z) = (-1, 1, 1) \text{ or } (1, -1, 1) \text{ or } (1, 1, -1), \\ +1 & \text{otherwise.} \end{cases} \end{aligned} \quad (3)$$

Using this detector function, we can easily prove the equivalence between stationarity and weak balance. That is, if Eq. (2) is true everywhere, it is straightforward to see that $W(\sigma_{ij}, \sigma_{jk}, \sigma_{ik}) = +1$, which proves that stationarity implies weak balance. In addition, for each of the five cases where $W(\sigma_{ij}, \sigma_{jk}, \sigma_{ik}) = +1$, we find that $\sigma'_{ij} = \sigma_{ij}$, hence the stationarity.

B. Cluster dynamics

To describe a group structure in mathematical terms, we define a cluster as a strongly connected component with respect to positive links. The size of a cluster is equal to the

number of vertices inside it. According to the structure theorem [17, 18], a balanced configuration in a complete graph consists of two clusters that have only negative links in between. One of the clusters may be of size zero, in which case the system has reached ‘paradise’ where only positive links exist. For weak balance, the corresponding structure theorem does not restrict the number of clusters, so a weakly balanced configuration in a complete graph can be divided into an arbitrary number of clusters in such a way that every two vertices belonging to different clusters are connected by negative links [20]. If we are interested in the average number of clusters or the distribution of cluster sizes, such information should be obtained by analyzing the cluster dynamics induced by Eq. (1).

To obtain a basic picture of the cluster dynamics under judging, assume that we have a weakly balanced configuration composed of three clusters as denoted below:

$$C = \{\{v_1, \dots, v_{n-1}, v_n\}, \{v_{n+1}, \dots, v_{n+m}\}, \{v_{n+m}, \dots, v_N\}\}. \quad (4)$$

When v_n makes a mistake by regarding one of its friends, say, v_1 , as bad, the system can either return back to the original configuration C in the end, or arrive at another weakly balanced configuration

$$C' = \{\{v_1, \dots, v_{n-1}\}, \{v_n\}, \{v_{n+1}, \dots, v_{n+m}\}, \{v_{n+m}, \dots, v_N\}\}, \quad (5)$$

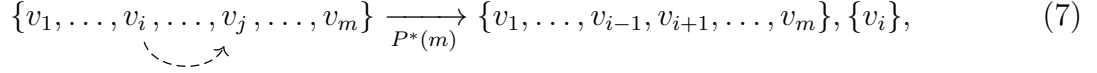
in which v_n forms a new cluster by itself. If v_n in Eq. (4) makes a different kind of mistake by regarding an enemy, say, v_{n+1} , as good, the final configuration can be either C or C' or

$$C'' = \{\{v_1, \dots, v_{n-1}\}, \{v_n, v_{n+1}, \dots, v_{n+m}\}, \{v_{n+m}, \dots, v_N\}\}. \quad (6)$$

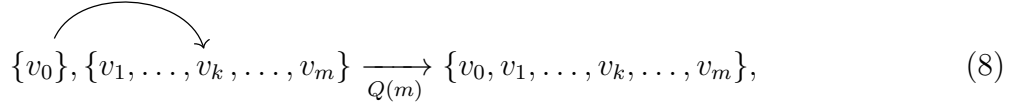
The process from C to C' will be called division, and the other one from C to C'' will be called migration henceforth. Note that the last cluster denoted by $\{v_{n+m}, \dots, v_N\}$ represents all the clusters that are not involved in the mistake committed by v_n , and it turns out that they remain bystanders throughout the subsequent process. This implies that we may focus only on the clusters involved with the error during every single process.

Every time the system reaches a weakly balanced configuration through judging, we introduce another assessment error at a random link to let it escape from this absorbing state. Thus, each assessment error defines the unit of time in this dynamics among weakly balanced configurations. More precisely speaking, if ϵ denotes the probability of assessment error, the time scale $O(1/\epsilon)$ between two consecutive errors is assumed to be much longer than the typical time scale for the system to reach a weakly balanced configuration.

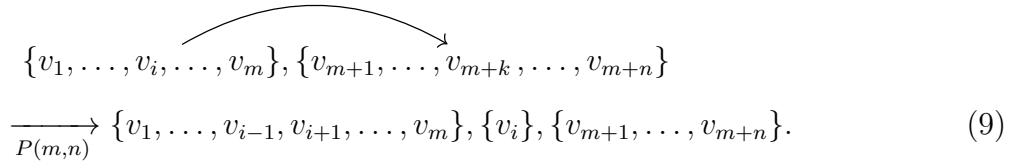
Let $P^*(m)$ denote the conditional probability that a vertex v_i in a cluster of size m separates from the others to form a new single-vertex cluster, given that it has committed an error toward a friend v_j in the same cluster, as illustrated by the following diagram:

$$\{v_1, \dots, v_i, \dots, v_j, \dots, v_m\} \xrightarrow{P^*(m)} \{v_1, \dots, v_{i-1}, v_{i+1}, \dots, v_m\}, \{v_i\}, \quad (7)$$


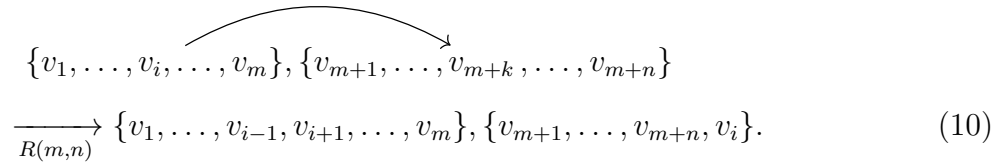
where the dashed arrow means the erroneous bad assessment. The inverse process is merging between a single-vertex cluster and another cluster with m vertices when the single vertex assesses one of its enemies, say, v_k , in the other cluster as good by mistake. Given that the mistake has occurred, the conditional probability of merging is denoted as $Q(m)$, and the process can be depicted as follows:

$$\{v_0\}, \{v_1, \dots, v_k, \dots, v_m\} \xrightarrow{Q(m)} \{v_0, v_1, \dots, v_k, \dots, v_m\}, \quad (8)$$


where the solid arrow means the erroneous good assessment. To describe the other route of division, $P(m, n)$ denotes the probability that a vertex v_i in a cluster of size m separates from the others to form a new single-vertex cluster, given that it has committed an error toward an enemy v_{m+k} in another cluster of size n . The process occurs as depicted below:

$$\begin{aligned} & \{v_1, \dots, v_i, \dots, v_m\}, \{v_{m+1}, \dots, v_{m+k}, \dots, v_{m+n}\} \\ & \xrightarrow{P(m,n)} \{v_1, \dots, v_{i-1}, v_{i+1}, \dots, v_m\}, \{v_i\}, \{v_{m+1}, \dots, v_{m+n}\}. \end{aligned} \quad (9)$$


The same kind of error may also lead to migration of the error-committing vertex v_i from the original cluster of size m to the other cluster of size n with probability $R(m, n)$ as follows:

$$\begin{aligned} & \{v_1, \dots, v_i, \dots, v_m\}, \{v_{m+1}, \dots, v_{m+k}, \dots, v_{m+n}\} \\ & \xrightarrow{R(m,n)} \{v_1, \dots, v_{i-1}, v_{i+1}, \dots, v_m\}, \{v_{m+1}, \dots, v_{m+n}, v_i\}. \end{aligned} \quad (10)$$


In Appendix A, we have proved $P^*(m) = Q(m-1) = 1/m$. In Appendix B, we have explained a numerically exact method for calculating $P(m, n)$ and $R(m, n)$. Figure 1 shows the results when $L \equiv m + n$ is fixed. Note that we have identified $R(1, L-1)$ with $Q(L-1) = 1/L$ because migration is effectively identical to merging if a single-vertex cluster is absorbed into another cluster. It is also worth noting that $P(m, L-m) \approx P^*(m) = 1/m$ when $m \gtrsim O(10)$.

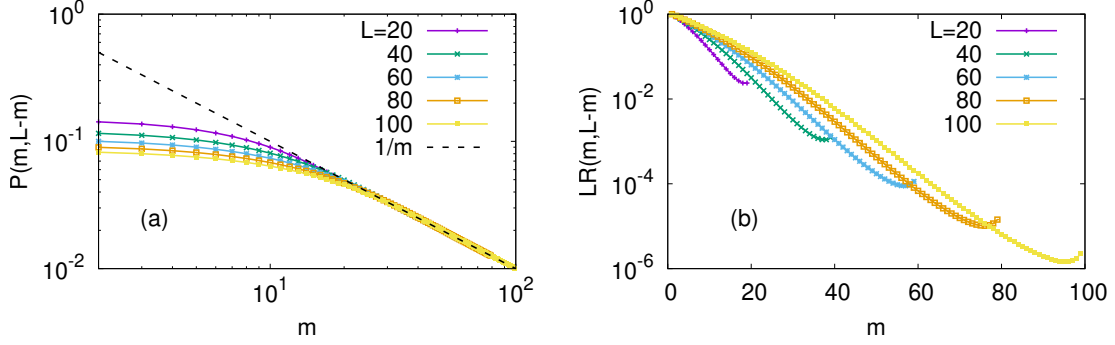


FIG. 1. (a) Probability of division [Eq. (9)] when $L \equiv m + n$ is fixed. We have depicted $P^*(m) = 1/m$ as a dashed line for comparison. (b) Probability of migration [Eq. (10)], multiplied by L to incorporate $R(1, L-1) \equiv Q(L-1) = 1/L$ as an end point.

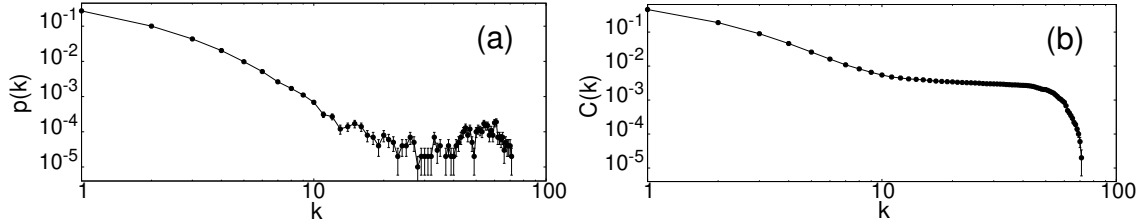


FIG. 2. (a) Steady-state cluster size distribution in a complete graph with $N = 100$ vertices. We initially start from a random configuration with an equal probability of positive and negative links and let it evolve according to the judging norm until it reaches a weakly balanced configuration. From then on, we attempt transitions among weakly balanced configurations according to the probabilities $P^*(m)$, $Q(m)$, $P(m, n)$, and $R(m, n)$ for 2×10^9 times. We have checked that the system converges to the same distribution regardless of the initial probability of positive links. The average has been taken over 10^3 samples. (b) The corresponding cumulative distribution $C(k) \equiv \int_k^\infty p(k') dk'$.

Using the probabilities of division, merging, and migration obtained above, we calculate the distribution of cluster sizes in a steady state (Fig. 2). Here, the probability of observing a cluster of size k is denoted by $p(k)$, and the normalization condition is given by $\sum_k kp(k) = 1$. In the language of percolation, the distribution suggests that the system is in a supercritical phase, where we find a giant cluster that occupies a finite fraction of the system. This analogy with percolation predicts that the overall frequency of good assessments will be low, although greater than zero, because we have positive links within a finite fraction of the

system. This prediction is indeed consistent with a recent study [29], in which the average frequency is found to be around 30% under judging in the presence of assessment error. This is even lower than that of stern judging, according to which every player can expect good assessments from its friends comprising 50% of the population.

IV. DISCUSSION

The bias toward giant clusters is already clear in Fig. 1(b), which implies that the probability of migration from a small cluster to a large one is exponentially higher than that of the opposite direction. However, the sizes of clusters can still be heterogeneous because the existence of a giant cluster implies the existence of smaller ones in the following sense: The probability that a giant cluster of size m loses one specific vertex is $O(1/m)$, and the number of vertices is m . In total, the giant cluster will divide at a constant rate, and this process will form a dynamic equilibrium with the migration toward the giant cluster.

Such a distribution as in Fig. 2 is not hard to find in society. One of the most common examples of antagonistic group structure would be the formation of political parties [30, 31]. In fact, politics is closely related to moral judgments, and empirical studies suggest that political orientations are even more stable than moral intuitions [32, 33]. We propose that stern judging and judging describe the cluster dynamics of the presidential system and that of the parliamentary system, respectively. The winner-take-all situation in the presidential system [34, 35] is well characterized by the proposition that an enemy’s enemy is a friend, whereas such pressure should be weaker in the parliamentary system. In Fig. 3, we show the respective cumulative distributions of seats in the parliaments of Germany, the United Kingdom, and Spain [36], which have the largest parliaments among European countries with high human freedom scores [37]. Although the distributions are broad, the bumps in large k indicate the existence of giant clusters. Our proposal thus explains the stability of the two-party system in the presidential system, as is observed in the United States, at the level of social norms, and the idea can be extended to the parliamentary system.

Let us add that stationarity is equivalent to weak balance in another social norm called ‘staying’ (also known as L7). It is different from judging (L8) only by $\alpha_{GCB} = G$. Considering the same difference between L4 and L6 (stern judging), we can say that L7 (staying) is for L8 (judging) what L4 is for L6 (stern judging). In fact, under L7 (staying), the system arrives at

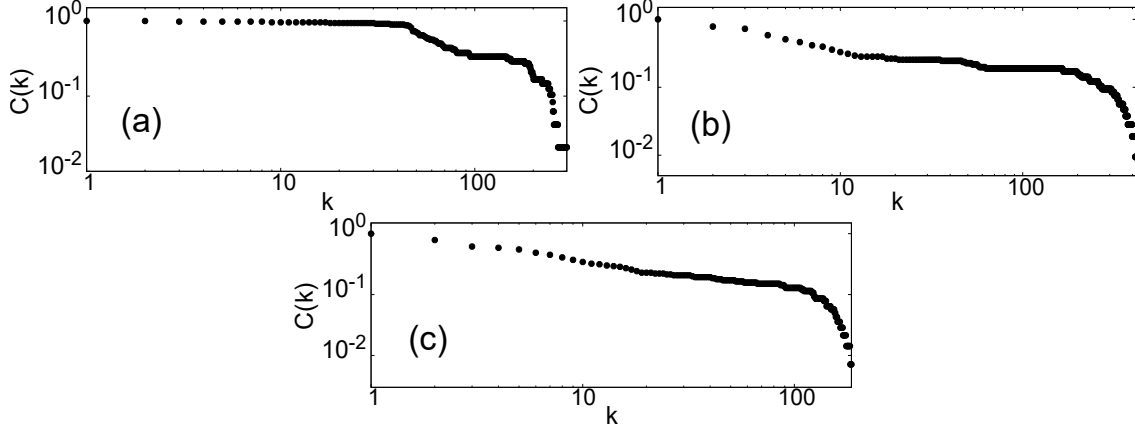


FIG. 3. (a) Cumulative distribution of seats in the parliament of Germany from 1990 to 2017, during which it had eight elections. The plateau at $k \lesssim 50$ may be due to the electoral threshold, which bars small parties from access to the parliament. (b) The case of the United Kingdom from 1983 to 2019, during which it had 10 elections. (c) The case of Spain from 1989 to 2020, during which it had 11 elections.

paradise in a way similar to L4 [16]. However, this is not as trivial as it looks at first glance if we think of the fact that the paradise is only neutrally stable under staying when viewed from a continuous model of indirect reciprocity, which treats each player’s assessment and cooperation level as continuous variables [38, 39]. Likewise, the stable fixed point of judging is the total absence of cooperation according to the continuous model [40], in contrast to the finite probability of cooperation observed in this work. This marked difference of the continuous model from the conventional discrete one would be an interesting question to be explored in the future.

V. SUMMARY

In summary, we have studied the mean-field dynamics of judging, as defined in the field of indirect reciprocity, on complete graphs. We have proved that this dynamics becomes stationary if and only if the configuration satisfies the weak form of structural balance. The weak balance is widely observed in empirical social networks when they consist of multiple antagonistic groups, and our study offers a simple mechanism to achieve it based on the interaction of a donor, a recipient, and observers. When assessment errors occur with a small probability, the system may escape from a weakly balanced configuration with the

aid of an error and end up with another weakly balanced configuration before the next assessment error occurs. We have calculated the corresponding transition probability from one cluster configuration to another in a numerically exact way. The resulting steady-state distribution of cluster sizes shows the coexistence of a giant cluster and smaller ones, as seen in the supercritical phase in percolation. For a real-life example, this is comparable to the size distribution of political parties in the parliamentary system. Our suggestion is that the cluster dynamics of judging and stern judging correspond to the parliamentary system and the presidential system, respectively. Furthermore, if α_{GCB} is changed from B to G , we can say that the most probable configuration becomes paradise instead of the one segregated into multiple clusters that are hostile to each other. This suggests how a small change in a social norm can induce macroscopic changes throughout the social network.

ACKNOWLEDGMENTS

M.B. and S.K.B. acknowledge support by Basic Science Research Program through the National Research Foundation of Korea (NRF) funded by the Ministry of Education (NRF-2020R1I1A2071670).

-
- [1] J. K. Hamlin, K. Wynn, and P. Bloom, *Nature* **450**, 557 (2007).
 - [2] F. Ting and R. Baillargeon, *Proc. Natl. Acad. Sci. USA* **118**, e2109045118 (2021).
 - [3] M. A. Nowak and K. Sigmund, *Nature* **393**, 573 (1998).
 - [4] H. Ohtsuki and Y. Iwasa, *J. Theor. Biol.* **231**, 107 (2004).
 - [5] M. A. Nowak and K. Sigmund, *Nature* **437**, 1291 (2005).
 - [6] H. Ohtsuki and Y. Iwasa, *J. Theor. Biol.* **239**, 435 (2006).
 - [7] C. Hilbe, L. Schmid, J. Tkadlec, K. Chatterjee, and M. A. Nowak, *Proc. Natl. Acad. Sci. USA* **115**, 12241 (2018).
 - [8] J. M. Pacheco, F. C. Santos, and F. A. C. Chalub, *PLoS Comput. Biol.* **2**, e178 (2006).
 - [9] F. P. Santos, F. C. Santos, and J. M. Pacheco, *Nature* **555**, 242 (2018).
 - [10] F. P. Santos, J. M. Pacheco, and F. C. Santos, *Philos. Trans. R. Soc. B* **376**, 20200291 (2021).
 - [11] Y. Fujimoto and H. Ohtsuki, *Sci. Rep.* **12**, 10500 (2022).

- [12] Y. Fujimoto and H. Ohtsuki, Proc. Natl. Acad. Sci. USA **120**, e2300544120 (2023).
- [13] F. Heider, J. Psychol. **21**, 107 (1946).
- [14] K. Oishi, T. Shimada, and N. Ito, Phys. Rev. E **87**, 030801(R) (2013).
- [15] K. Oishi, S. Miyano, K. Kaski, and T. Shimada, Phys. Rev. E **104**, 024310 (2021).
- [16] M. Bae, T. Shimada, and S. K. Baek, Phys. Rev. E **110**, L052301 (2024).
- [17] F. Harary, Mich. Math. J. **2**, 143 (1953).
- [18] D. Cartwright and F. Harary, Psychol. Rev. **63**, 277 (1956).
- [19] S. A. Marvel, J. Kleinberg, R. D. Kleinberg, and S. H. Strogatz, Proc. Natl. Acad. Sci. USA **108**, 1771 (2011).
- [20] D. Easley and J. Kleinberg, “A weaker form of structural balance,” in *Networks, Crowds, and Markets: Reasoning about a Highly Connected World* (Cambridge University Press, Cambridge, 2010) Chap. 5, pp. 115–118.
- [21] M. Szell, R. Lambiotte, and S. Thurner, Proc. Natl. Acad. Sci. USA **107**, 13636 (2010).
- [22] J. Leskovec, D. Huttenlocher, and J. Kleinberg, in *Proc. SIGCHI Conf. Hum. Factor Comput. Syst.* (Association for Computing Machinery, New York, NY, 2010) pp. 1361–1370.
- [23] A. Ilany, A. Barocas, L. Koren, M. Kam, and E. Geffen, Anim. Behav. **85**, 1397 (2013).
- [24] K. Malarz and J. A. Hołyst, Phys. Rev. E **106**, 064139 (2022).
- [25] M. Wołoszyn and K. Malarz, Phys. Rev. E **105**, 024301 (2022).
- [26] K. Malarz and M. Wołoszyn, Chaos **33**, 073115 (2023).
- [27] K. Kułakowski, P. Gawroński, and P. Gronek, Int. J. Mod. Phys. C **16**, 707 (2005).
- [28] H. Brandt, H. Ohtsuki, Y. Iwasa, and K. Sigmund, in *Mathematics for Ecology and Environmental Sciences*, edited by Y. Takeuchi, Y. Iwasa, and K. Sato (Springer, 2007) Chap. 3, pp. 21–49.
- [29] Y. Fujimoto and H. Ohtsuki, PRX Life **2**, 023009 (2024).
- [30] S. K. Baek, J. Kim, S. S. Lee, W. S. Jo, and B. J. Kim, Physica A **560**, 125178 (2020).
- [31] J. Kim and S. K. Baek, J. Korean Phys. Soc. **80**, 509 (2022).
- [32] P. K. Hatemi, C. Crabtree, and K. B. Smith, Am. J. Political Sci. **63**, 788 (2019).
- [33] B. N. Bakker, Y. Lelkes, and A. Malka, Am. Political Sci. Rev. **115**, 1482 (2021).
- [34] S. K. Baek, S.-W. Son, and H.-C. Jeong, Phys. Rev. E **91**, 042144 (2015).
- [35] J. Kim, H.-C. Jeong, and S. K. Baek, Physica A **607**, 128207 (2022).
- [36] A. Fontan and C. Altafini, Sci. Rep. **11**, 5134 (2021).

- [37] Cato Institute, available at <https://www.cato.org/human-freedom-index/2023> (accessed 2024 Dec 30).
- [38] S. Lee, Y. Murase, and S. K. Baek, *Sci. Rep.* **11**, 14225 (2021).
- [39] S. Lee, Y. Murase, and S. K. Baek, *J. Theor. Biol.* **548**, 111202 (2022).
- [40] Y. Mun, Q. A. Le, and S. K. Baek, *J. Korean Phys. Soc.* **85**, 969–976 (2024).

Appendix A: Derivation of $P^*(m) = Q(m-1) = 1/m$

When an assessment error occurs in a cluster of size m , the transition between configurations forms a ladder structure [see Fig. A1(a) for $m = 5$]. For general m , we have Fig. A1(b), where

$$\mu_j \equiv \left(\frac{1}{m}\right) \left(\frac{m-j}{m}\right) \quad (\text{A1a})$$

$$\pi_j^+ \equiv \left(\frac{m-j}{m}\right) \left(\frac{j}{m}\right) \quad (\text{A1b})$$

$$\pi_j^- \equiv \left(\frac{j-1}{m}\right) \left(\frac{m-j}{m}\right) \quad (\text{A1c})$$

$$\nu_j \equiv \left(\frac{1}{m}\right) \left(\frac{j-1}{m}\right) \quad (\text{A1d})$$

$$\tau_j^+ \equiv \left(\frac{m-j}{m}\right) \left(\frac{j-1}{m}\right) \quad (\text{A1e})$$

$$\tau_j^- \equiv \left(\frac{j-1}{m}\right) \left(\frac{m-j+1}{m}\right). \quad (\text{A1f})$$

Each of observable configurations during the subsequent process is represented by a circle in Fig. A1(b), and the upper and lower circles are denoted by j and j' , respectively, where $j = 1, \dots, m$. Starting from one of those configurations, the probability of absorption into a fully separated configuration (represented by the upper rightmost circle, m) is denoted by q_j or $q_{j'}$ accordingly. The probabilities are related to each other by the following recursion formulas:

$$q_j = \mu_j q_{j'} + \pi_j^+ q_{j+1} + \pi_j^- q_{j-1} + (1 - \mu_j - \pi_j^+ - \pi_j^-) q_j \quad (\text{A2a})$$

$$q_{j'} = \nu_j q_j + \tau_j^+ q_{(j+1)'} + \tau_j^- q_{(j-1)'} + (1 - \nu_j - \tau_j^+ - \tau_j^-) q_{j'} \quad (\text{A2b})$$

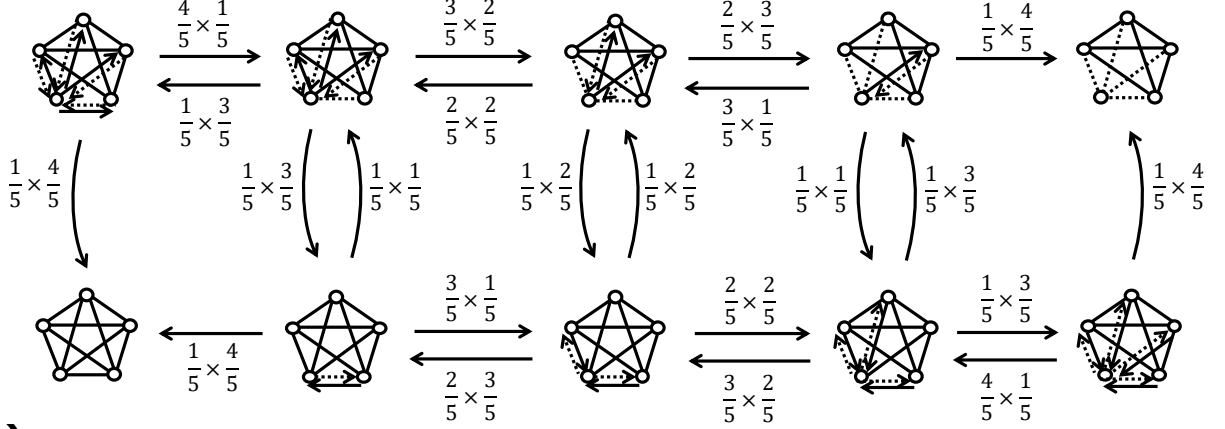
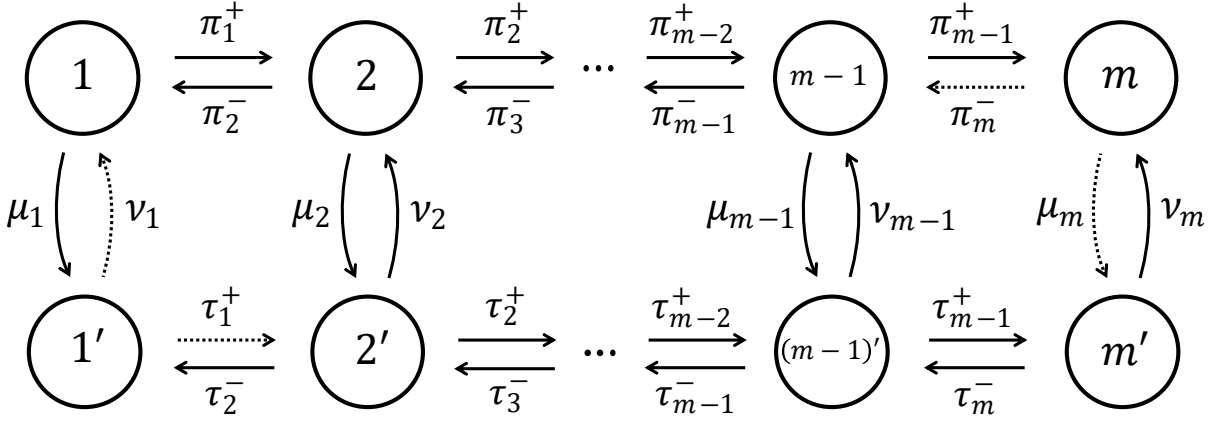
(a)**(b)**

FIG. A1. Transition structure when a cluster of size m is divided into two because of an internal error between its member vertices. (a) An example of $m = 5$, where each transition is represented by an arrow with its probability. In each configuration, solid and dotted arrows mean good and bad assessments, respectively. (b) Generalization to an arbitrary m . The transition probabilities are given in Eq. (A1), and we have drawn dotted arrows for ν_1 , τ_1^+ , π_m^- , and μ_m because the probabilities are actually zero.

with $q_{1'} \equiv 0$ and $q_m \equiv 1$. It is straightforward to verify that the above equations are satisfied by the following solution:

$$q_j = \frac{j}{m} \quad (\text{A3a})$$

$$q_{j'} = \frac{j-1}{m}. \quad (\text{A3b})$$

The conditional probability $P^*(m)$ that a vertex separates from its cluster of size m corresponds to $q_{2'} = 1/m$, whereas the merging probability is $Q(m-1) = 1 - q_{m-1} = 1/m$.

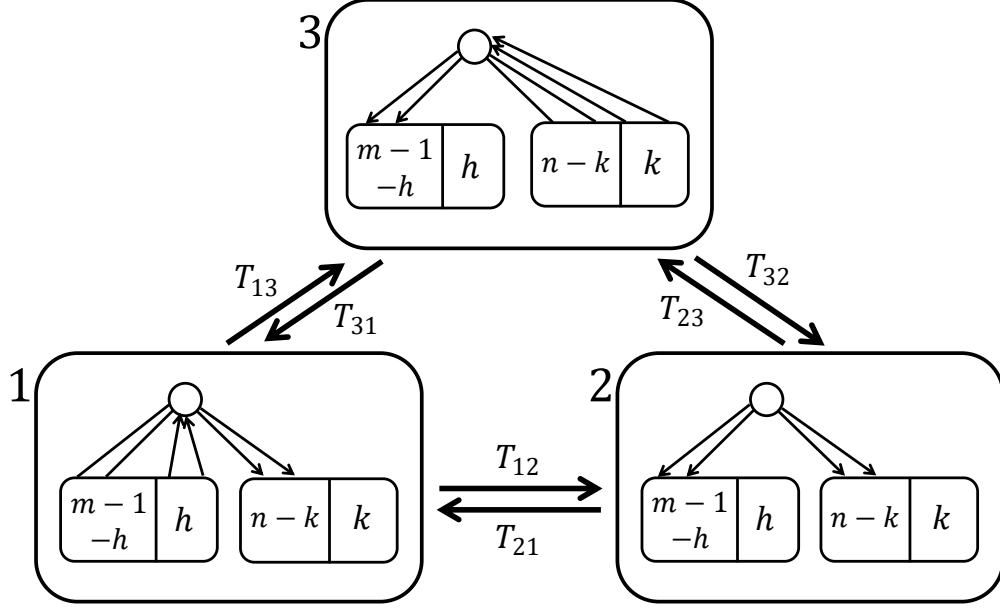


FIG. B1. A unit triangle for $0 \leq k \leq n - 1$ and $0 \leq h \leq m - 2$. The circle mean v_i in Eq. (5) or (6), who was a member of the m -sized cluster in the original configuration but committed an assessment error toward a member of the n -sized cluster. We have drawn only positive links, and the links without arrow heads are bidirectional. The transition probabilities are given in Eq. (B1).

Note that α_{BDB} , the only difference between L6 and L8, is not involved in this process at all, which means that $P^*(m) = Q(m - 1)$ due to the path-reversal symmetry [16].

Appendix B: Calculation of $P(m, n)$ and $R(m, n)$

Consider two clusters of respective sizes m and n with $m + n \leq N$, where N is the total number of vertices in the complete graph. If a member of the m -sized cluster, say, v_i , makes an error in assessing a member of the n -sized cluster, we have three accessible absorbing configurations: The first is the original. The second is such that v_i forms a new single-vertex cluster [Eq. (9)]. The last is such that v_i migrates to the n -sized cluster [Eq. (10)]. The probability of absorption into each of these configurations is calculated in a numerically exact manner, as will be explained below.

A crucial observation is the existence of a triangular unit consisting of the three configurations in Fig. B1, where the configurations can be visited with the following transition

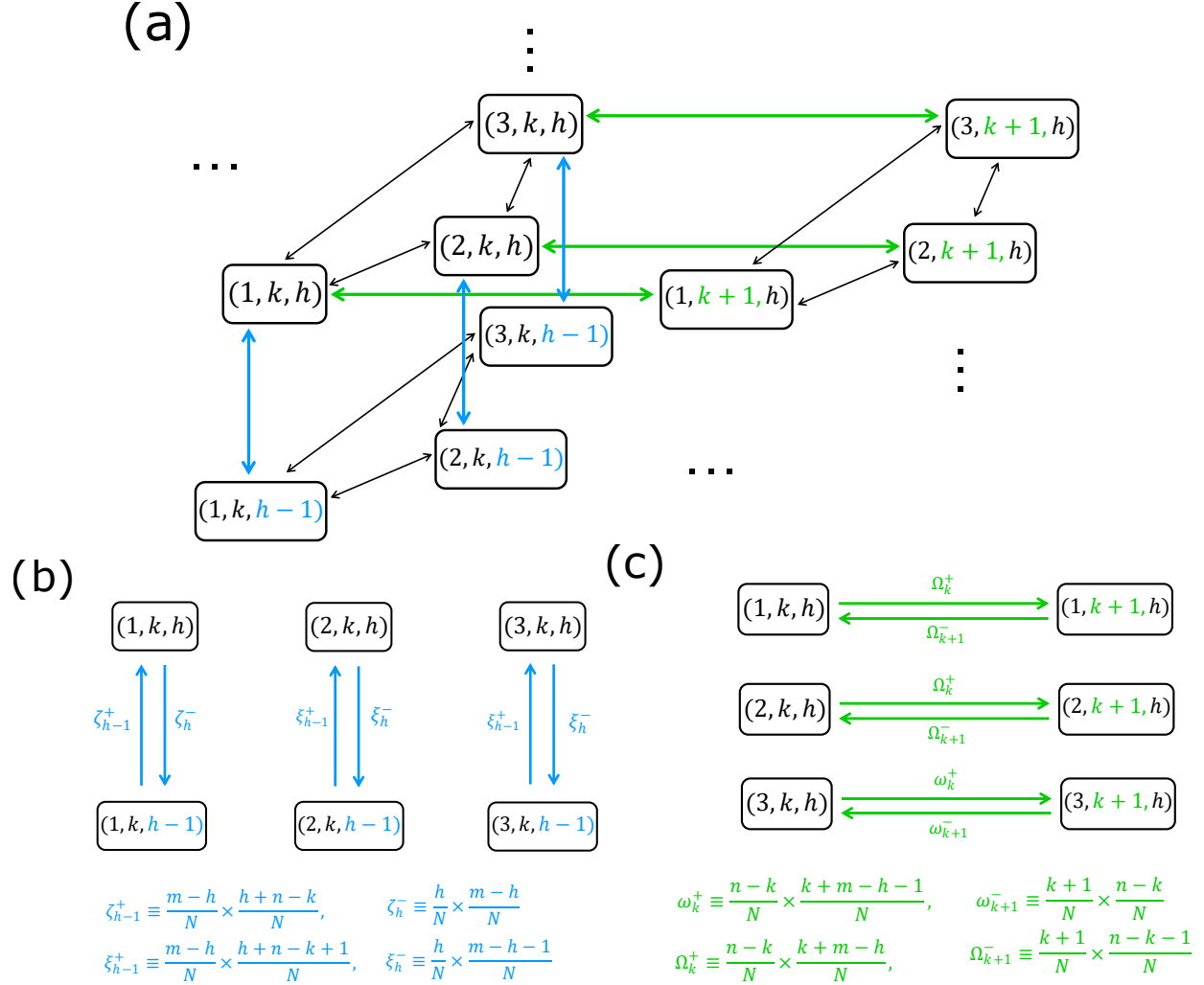


FIG. B2. (a) Three dimensional structure composed of triangular units such as in Fig. B1. (b) In the vertical direction, the unit triangle of $(1, k, h)$, $(2, k, h)$, and $(3, k, h)$ connects to other triangles having $h \pm 1$ with transition probabilities ζ_h^\pm or ξ_h^\pm . (c) In the horizontal direction, the unit triangle connects to other triangles having $k \pm 1$ with transition probabilities ω_k^\pm or Ω_k^\pm .

probabilities:

$$T_{12} = \frac{1}{N} \times \frac{h}{N} \quad (\text{B1a})$$

$$T_{21} = \frac{1}{N} \times \frac{m-1-h}{N} \quad (\text{B1b})$$

$$T_{23} = \frac{1}{N} \times \frac{n-k}{N} \quad (\text{B1c})$$

$$T_{32} = \frac{1}{N} \times \frac{k}{N} \quad (\text{B1d})$$

$$T_{31} = \frac{1}{N} \times \frac{m-1-h}{N} \quad (\text{B1e})$$

$$T_{13} = \frac{1}{N} \times \frac{n-k}{N}, \quad (\text{B1f})$$

where $0 \leq k \leq n-1$ and $0 \leq h \leq m-2$. This triangular unit can be characterized by two integers, h and k . As shown in Fig. B1, the three configurations can thus be indicated by $(1, k, h)$, $(2, k, h)$, and $(3, k, h)$. Then, such triangular units are connected to each other to form a three-dimensional structure as depicted in Fig. B2(a). In Fig. B2(b) and (c), we have written the transition probabilities connecting the triangular units, denoted as ζ_h^\pm , ω_k^\pm , and Ω_k^\pm . Consequently, the absorption probabilities are related to each other by the following set of linear equations:

$$\begin{aligned} q_{1,k,h} &= T_{12}q_{2,k,h} + T_{13}q_{3,k,h} + \Omega_k^- q_{1,k-1,h} + \Omega_k^+ q_{1,k+1,h} + \zeta_h^- q_{1,k,h-1} + \zeta_h^+ q_{1,k,h+1} \\ &+ (1 - T_{12} - T_{13} - \Omega_k^- - \Omega_k^+ - \zeta_h^- - \zeta_h^+) q_{1,k,h} \end{aligned} \quad (\text{B2a})$$

$$\begin{aligned} q_{2,k,h} &= T_{21}q_{1,k,h} + T_{23}q_{3,k,h} + \Omega_k^- q_{2,k-1,h} + \Omega_k^+ q_{2,k+1,h} + \xi_h^- q_{2,k,h-1} + \xi_h^+ q_{2,k,h+1} \\ &+ (1 - T_{21} - T_{23} - \Omega_k^- - \Omega_k^+ - \xi_h^- - \xi_h^+) q_{2,k,h} \end{aligned} \quad (\text{B2b})$$

$$\begin{aligned} q_{3,k,h} &= T_{31}q_{1,k,h} + T_{32}q_{2,k,h} + \omega_k^- q_{3,k-1,h} + \omega_k^+ q_{3,k+1,h} + \xi_h^- q_{3,k,h-1} + \xi_h^+ q_{3,k,h+1} \\ &+ (1 - T_{31} - T_{32} - \omega_k^- - \omega_k^+ - \xi_h^- - \xi_h^+) q_{3,k,h}. \end{aligned} \quad (\text{B2c})$$

We can obtain $P(m, n)$ and $Q(m, n)$ by solving this linear system. Note that the three-dimensional structure is bounded by the ladder-shaped modules analyzed in Appendix A. One module is for a cluster of size m , and the other is for a cluster of size $(n+1)$. The absorption probability of each configuration inside the modules [Eq. (A3)] thus defines the boundary conditions of this three-dimensional random-walk problem with absorbing boundaries. Let us decompose the boundary conditions into three parts. The first is for $(1, k, h)$: if $k = n$, $(1, k, h)$ is mapped to a configuration that can be denoted by $(h+1)'$ in analyzing the cluster of size m . This is what we mean by “ $(h+1)'$ for $P^*(m)$ ” in Fig. B3. In addition,

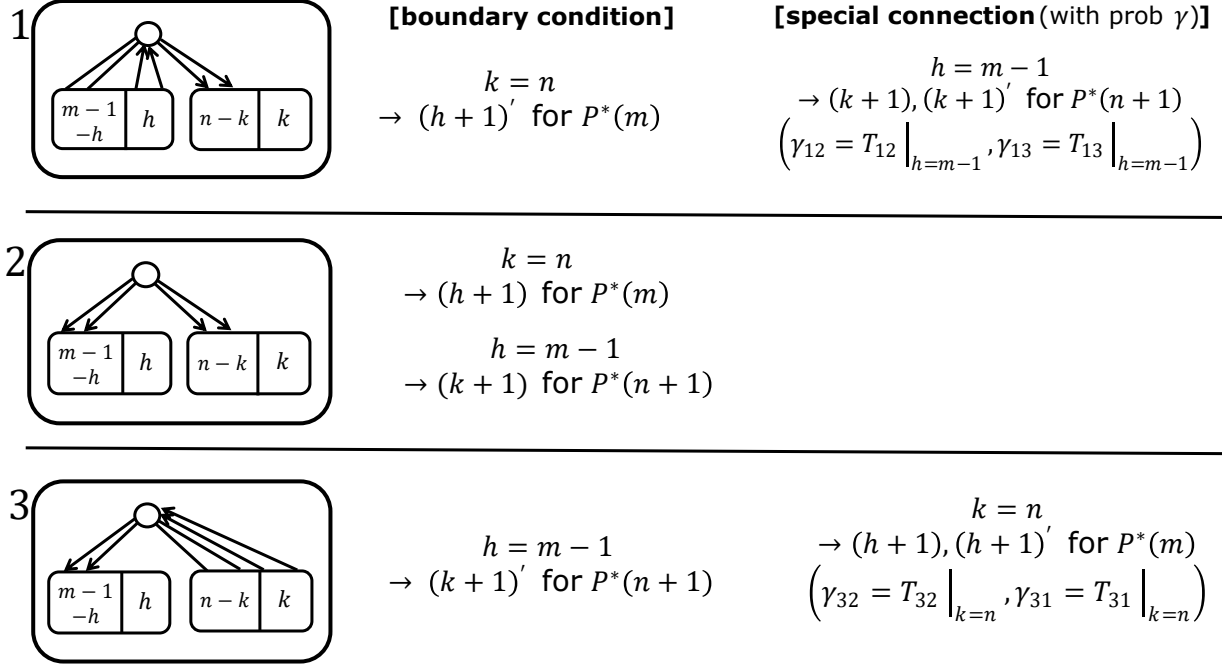


FIG. B3. Boundary conditions of the three-dimensional structure in Fig. B2. As in Fig. B1, we have depicted only positive links, and those with arrow heads are bidirectional links.

if $h = m - 1$, the system starting from $(1, k, h)$ can transit to $(k + 1)$ for $P^*(n + 1)$ with probability $\gamma_{12} = T_{12}|_{h=m-1}$, or to $(k + 1)'$ for $P^*(n + 1)$ with probability $\gamma_{13} = T_{13}|_{h=m-1}$. The second part of the boundary conditions is for $(2, k, h)$: It corresponds to $(h + 1)$ for $P^*(m)$ if $k = n$, and $(k + 1)$ for $P^*(n + 1)$ if $h = m - 1$. Finally, if $h = m - 1$, $(3, k, h)$ corresponds to $(k + 1)'$ for $P^*(n + 1)$. In addition, if $k = n$, the system starting from $(3, k, h)$ can transit to $(h + 1)$ for $P^*(m)$ with probability $\gamma_{32} = T_{32}|_{k=n}$, or to $(h + 1)'$ for $P^*(m)$ with probability $\gamma_{31} = T_{31}|_{k=n}$.

Figure B4 compares the transition probabilities obtained in this way and Monte Carlo estimates from agent-based simulations. Even when the size of a cluster is only $O(10)$, the transition probabilities are so small that the Monte Carlo estimates become highly imprecise [Fig. B4(f) and (h)].

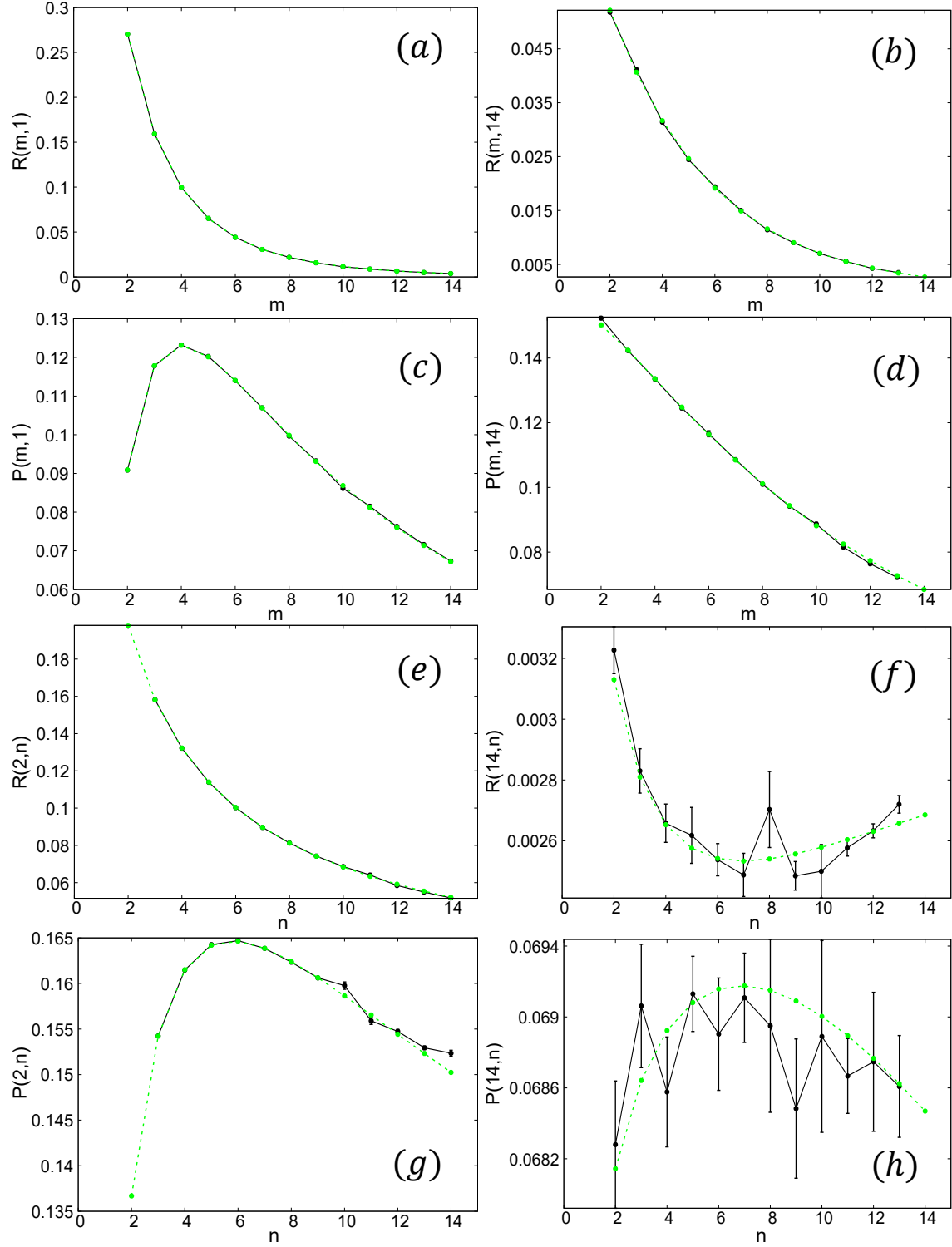


FIG. B4. Numerical confirmation of the transition probabilities calculated in Appendix B. The black solid lines have been obtained from agent-based simulations according to the judging norm (Table I), and the green dotted lines show our numerically exact results.